UNIVERSITY *of* York

This is a repository copy of *Measurement of fission-fragment mass distributions in the multinucleon transfer channels of the $^{18}O+^{237}Np$ reaction*.

White Rose
university consortium
Universities of Leeds, Sheffield & York

eprints@whiterose.ac.uk
https://eprints.whiterose.ac.uk/

Measurement of fission fragment mass distributions in the multi-nucleon transfer channels of the ^{18}O+^{237}Np reaction

M.J. Vermeulen[1], K. Nishio[1],[*] K. Hirose[1], K.R. Kean[2,1], H. Makii[1], R. Orlandi[1], K. Tsukada[1],
I. Tsekhanovich[3], A.N. Andreyev[4,1], S. Ishizaki[5], M. Okubayashi[5], S. Tanaka[5,1], and Y. Aritomo[5]

[1] *Advanced Science Research Center, Japan Atomic Energy Agency, Tokai, Ibaraki 319-1195 Japan*
[2] *Laboratory for Advanced Nuclear Energy, Institute for Innovative Research,*
and Department of Trans-disciplinary Science and Engineering, School of Environment and Society,
Tokyo Institute of Technology, Ookayama, Meguro-ku, Tokyo 152-8550, Japan
[3] *CENBG, CNRS/IN2P3-Université de Bordeaux, 33170 Gradignan, France*
[4] *Department of Physics, University of York, York YO10 5DD, United Kingdom and*
[5] *Graduate School of Science and Engineering, Kindai University, Higashi-Osaka 577-8502, Japan*

Fission fragment mass distributions for 23 nuclei ($^{234-237}$U, $^{236-239}$Np, $^{238-241}$Pu, $^{240-243}$Am, $^{242-245}$Cm, and $^{244-246}$Bk) were measured using the multi-nucleon transfer approach in the reaction of ^{18}O+^{237}Np, and their excitation-energy dependence was obtained up to a maximum of 70 MeV. Among them, the low energy fission of ^{236}Np, ^{238}Pu, and ^{245}Cm is reported for the first time. The experimental data for all the studied nuclei were compared to the Langevin calculations. The calculation which takes into account the effects of multi-chance fission well reproduced the peak-to-valley ratio and mass-asymmetric peak positions of the distributions. The angular momenta given to the fissioning nucleus is also discussed.

PACS numbers: 25.85.w, 25.70.Hi, 25.85.Ge, 27.90.+b

I. INTRODUCTION

Experimental data on the fission fragment mass distribution (FFMD) are the ingredients of primary importance for fission theory and are crucial for many applications including usage of atomic energy. We have recently developed a method to obtain FFMDs using the multi-nucleon transfer (MNT) channels available when bombarding actinide target nuclei with an ^{18}O beam [1, 2]. This unique approach can produce a variety of fission data for several nuclides as a function of excitation energy in one reaction at a single beam energy setting, which allows for investigation of multi-chance fission, see e.g. [2, 3]. The advantage of the MNT-reaction technique in normal kinematics is that it has the potential to extend fission data towards neutron-rich heavy-element nuclei which is currently not possible in experiments in inverse kinematics, such as SOFIA at GSI [4–6] and the VAMOS setup at GANIL [7–10], relying on the use of accelerated ^{238}U beam. For example, by the use of heavy exotic target material ^{254}Es, we can study fission in the fermium region where a sharp transition from an asymmetric to symmetric fission modes happens in ^{257}Fm and ^{258}Fm nuclei [11].

In this article, we report a measurement of FFMDs for nuclei produced in the ^{18}O+^{237}Np reaction which extends the series of previously conducted experiments [1, 2]. The FFMDs of 23 nuclides ($^{234-237}$U, $^{236-239}$Np, $^{238-241}$Pu, $^{240-243}$Am, $^{242-245}$Cm, and $^{244-246}$Bk) have been obtained at the excitation energy range up to 70 MeV. Among them fission of ^{236}Np, ^{238}Pu, and ^{245}Cm is reported for the first time. The present data set contains several nuclei that have already been studied by us in the ^{18}O+^{232}Th [1] and/or ^{18}O+^{238}U [2] reactions. Therefore it becomes now possible to examine the effect of different transfer channels on the FFMDs, these results will be discussed in this article.

Recently, Langevin calculations have been extensively adopted for the study of low-energy fission [3, 12–20]. In particular, thanks to the high predictive power for the FFMD calculation, the Langevin approach was used to discuss the importance of the multi-chance fission at high excitation energies [2, 3]. In this article, we calculated the FFMDs for all nuclei studied in this work. The calculation was extended to include the angular momentum of fissioning nucleus which is a sensitive parameter influencing the probability for each fission chance, thus allowing to estimate its impact on the FFMDs.

II. EXPERIMENTAL METHODS AND RESULTS

The experiment was performed at the JAEA tandem accelerator facility using a 162.0-MeV ^{18}O beam ($E_{\rm c.m.}$=150.5 MeV) with an intensity of $\sim$0.5 pnA. The target was prepared by electrodeposition of a 75 μg/cm^2 layer of ^{237}Np on a 300 μg/cm^2 nickel backing. The experimental setup is almost the same as in [1, 2], so only the most pertinent details will be described here. The setup consists of a multidetector ΔE-E silicon telescope, to detect ejectiles, and four multiwire proportional counters (MWPCs), to detect fission fragments.

Specific particle-transfer channels were determined by identifying the ejectiles using the ΔE-E silicon telescope. An ejectile passing through one of the twelve ΔE detec-
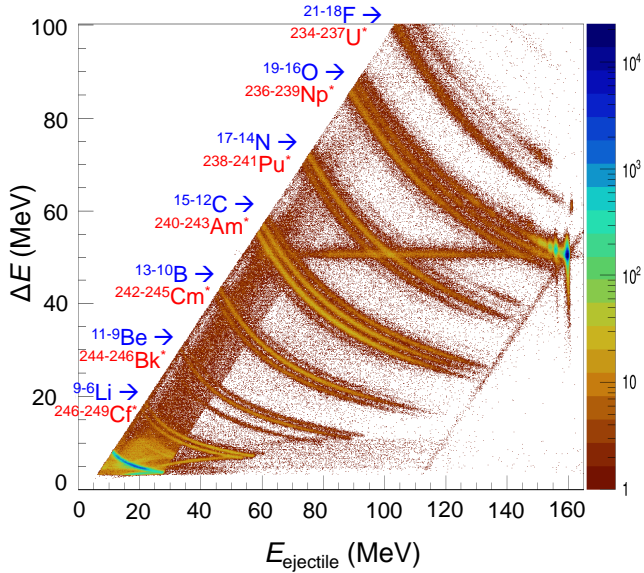
FIG. 1: (Color online) An example of identification of ejectile nuclei (labeled in blue) by the silicon ΔE-E telescope (data collected in one ΔE segment and one E strip only) obtained in the ^{18}O+^{237}Np reaction. The corresponding fissioning compound nuclei are shown in red.

tors (75 μm thick) is stopped in the 16-strip annular E detector (300 μm thick) to measure the residual energy ($E_{\rm res}$). Thus, the ejectile kinetic energy $E_{\rm ejectile}$ is represented by $\Delta E + E_{\rm res}$. The direction of a scattered ejectile was determined by the combination of a ΔE segment and one of the strips in the E detector.

Considering the binary kinematics event-by-event, the method allows to determine the total excitation energy of the exit channel $E_{\rm tot}^*$, as being the sum of the excitation energy of the fissioning nucleus and of the ejectile. Fission-fragment masses were deduced using the momentum conservation, where the velocity and direction of the recoiled fissioning nucleus were determined using the information on the coincident ejectile nuclide. Good energy resolution of the ΔE detectors, achieved using silicon wafers of highly uniform thickness ($<1.3\%$ variation), has allowed us to distinguish not only the ejectiles of different elements (e.g. F, O, N, C, B, Be, Li), but also different isotopes of each element, as shown in Fig. 1. In this figure, ejectiles of $^{21-18}$F, $^{19-16}$O, $^{17-14}$N, $^{15-12}$C, $^{13-10}$B, and $^{11-9}$Be are cleanly separated, corresponding to the population of the excited recoiled nuclei of $^{234-237}$U*, $^{236-239}$Np*, $^{238-241}$Pu*, $^{240-243}$Am*, $^{242-245}$Cm*, and $^{244-246}$Bk*, respectively, whose fission was studied in the present work. We also see the signature of fissioning nuclei $^{246-249}$Cf* (corresponding to the $^{9-6}$Li ejectiles). As the thickness of the annular E-detector was insufficient to stop the $^{9-6}$Li ejectiles, the respective data set was not evaluated.

Figure 2 shows the yields of fission fragments as a function of their mass and of the total excitation energy of the system ($E_{\rm tot}^*$). The fragment masses were deter-

mined with a resolution $\sigma_{\rm A}$=6.5 u. The data were derived from the analysis of coincidences between two FFs and an ejectile. It is clearly seen that the nuclei $^{234-237}$U, $^{236-239}$Np, $^{238-241}$Pu, and $^{240-241}$Am show a dominant mass-asymmetric fission mode. This is because, for the mentioned nuclei, the bulk of the measured data falls into a rather low excitation-energy range of $E_{\rm tot}^*\sim$10–40 MeV. Indeed, the $E_{\rm tot}^*$ distributions (red solid lines in Fig. 2), obtained by projecting the $E_{\rm tot}^*$–FF mass plots on the $E_{\rm tot}^*$-axis, have the maxima around 10-45 MeV. In contrast to this, the heavier fissioning nulclides, $^{242-243}$Am, $^{242-245}$Cm and $^{244-246}$Bk, exhibit a symmetric shape, primarily because the data were recorded only in the higher-excitation energy region of $E_{\rm tot}^*$>30 MeV. The latter is clearly demonstrated by the respective projections on $E_{\rm tot}^*$ in Fig. 2. As the proton and neutron number of the fissioning nucleus increases, $^{238-241}$Pu*($+1p+xn$) $\rightarrow$ $^{240-243}$Am*($+2p+xn$) $\rightarrow$ $^{242-245}$Cm*($+3p+xn$) $\rightarrow$ $^{244-246}$Bk*($+4p+xn$), the system tends to have a larger excitation energy on average, with a significant drop of the yield in the low-excitation energy region. This behaviour will be discussed in Section III A. Note that the abrupt drop of the yield populating the uranium nuclei ($^{234-237}$U*, $-1p\pm xn$ channels) at $E_{\rm tot}^*\geq$55 MeV is due to the fact that the low-energy fluorine isotopes are stopped in the ΔE detector, thus truncates the deduced excitation-energy distribution.

In the very low-energy region of the $E_{\rm tot}^*$ spectra in Fig. 2, $^{234-237}$U, ^{236,238,239}Np, $^{238-240}$Pu, and ^{240,241}Am show a sudden drop in the yield due to the fission barrier, marked by the arrows in Fig. 2. The fission barriers labeled by the magenta arrows are taken from the RIPL-3 library [21], and those by the blue arrows obtained in our MNT approach [22]. The drop associated with fission barrier is not visible for ^{237}Np due to a chance coincidence of fragments with strong elastic scattering events, as found in the strong yield at zero excitation energy of the channel ^{237}Np*. The structure originating from the fission barrier is invisible for ^{242,243}Am and $^{242-245}$Cm because of the low statistics arising from the MNT reaction mechanism and presence of non-negligible number of random coincidence events.

The FFMDs for the studied nuclei and their $E_{\rm tot}^*$ dependence are shown in Fig. 3. Here, the excitation-energy binning is chosen to be $\Delta E_{\rm tot}^*$ =10 MeV, and the yield is normalized so that the total area becomes 200 %. At the lowest excitation-energy bin of 7.0–20.0 MeV, the FFMDs show a predominantly asymmetric shape for all studied nuclei. The double-peak structure of the FFMD gradually smears out at higher excitation energies, and the shape becomes nearly mass-symmetric with a Gaussian-like distribution. The systematic change of the FFMDs with respect to the mass and atomic number of the fissioning nucleus, as well as their evolution with excitation energy, is discussed in the next section.
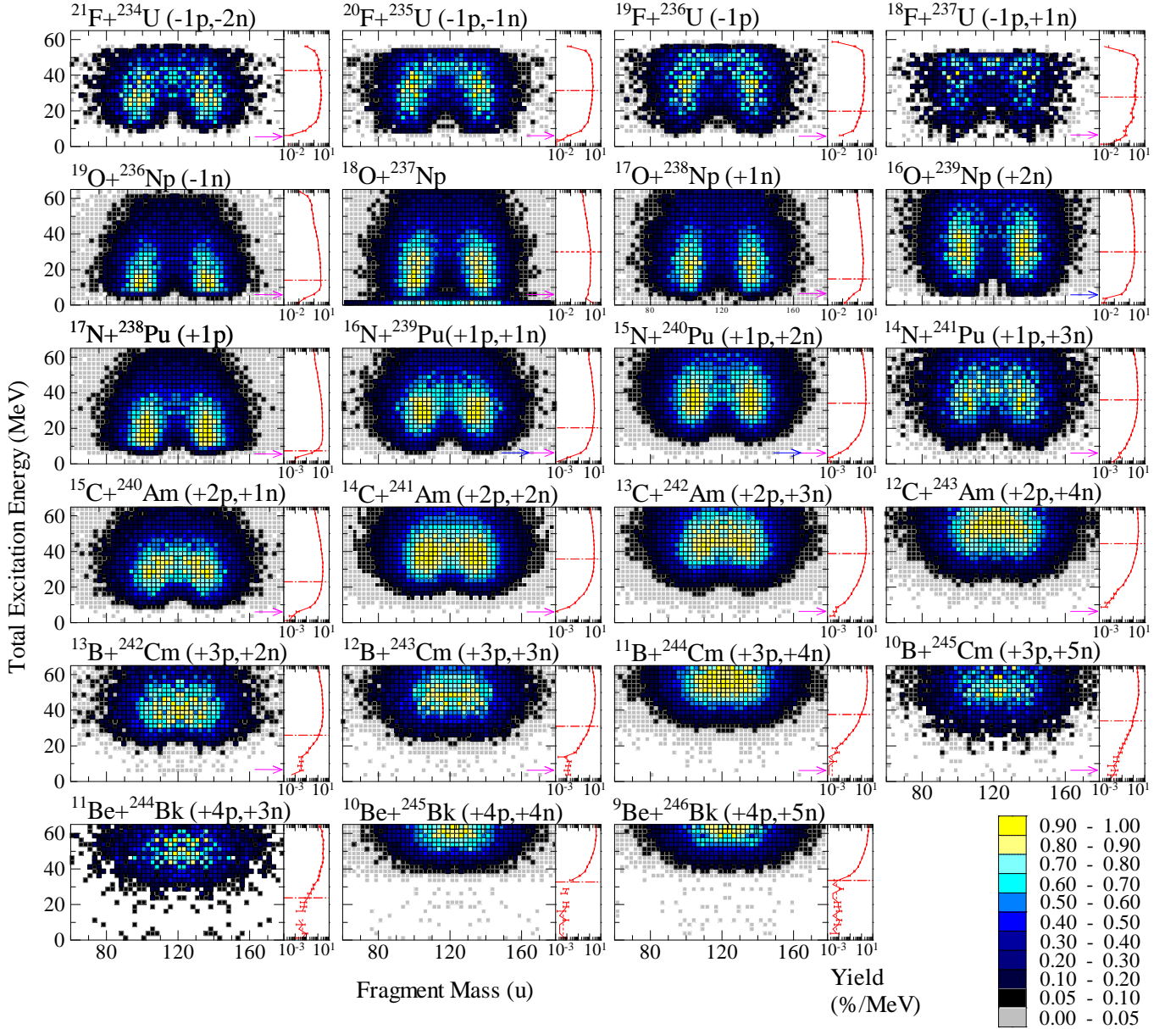
FIG. 2: (Color online) The yield of fission fragments as a function of their mass and total excitation energy (E^*_{tot}), obtained for each MNT channel. The solid red lines with error bars plotted on the right-side panel of each channel provide the projection from E^*_{tot}–FF plot on the E^*_{tot} axis. Here, the projected spectra are normalized so that the total area accumulated in the excitation-energy range $0 < E^*_{\mathrm{tot}} < 65$ MeV becomes 100%. The horizontal dash-dotted line in the right-side panel shows the most probable total excitation energy E^*_{opt} calculated using the momentum matching condition (see Table I and Section III A). Fission barrier heights B_{f} from the RIPL3 library [21] are shown by the magenta arrows, where B_{f} values of ^{234,235,236}U correspond to the outer barrier of the double-humped fission barrier and others refer the inner barrier. Barrier data of ^{239}Np, ^{239}Pu and ^{240}Pu derived by the MNT approach in [22] are shown by the blue arrows.

III. DISCUSSIONS

A. Most probable total excitation energy

The trend of excitaion energy distributions shown in Fig. 2 will be examined more quantitatively using a calculation based on the momentum matching condition [23–25].

The excitation-energy distributions in Fig. 2 were derived from the coincidence spectra between ejectile and fission fragments, thus they represent the quantity proportional to the probability to create a compound nucleus (CN) with excitation energy E^*, $P_{\mathrm{CN}}(E^*)$, multiplied by the fission probability $P_{\mathrm{f}}(E^*)$. As the excitation function of P_{f} is nearly constant above $E^* \gtrsim 10$ MeV [26], the shape of the excitation-energy distribution in Fig. 2
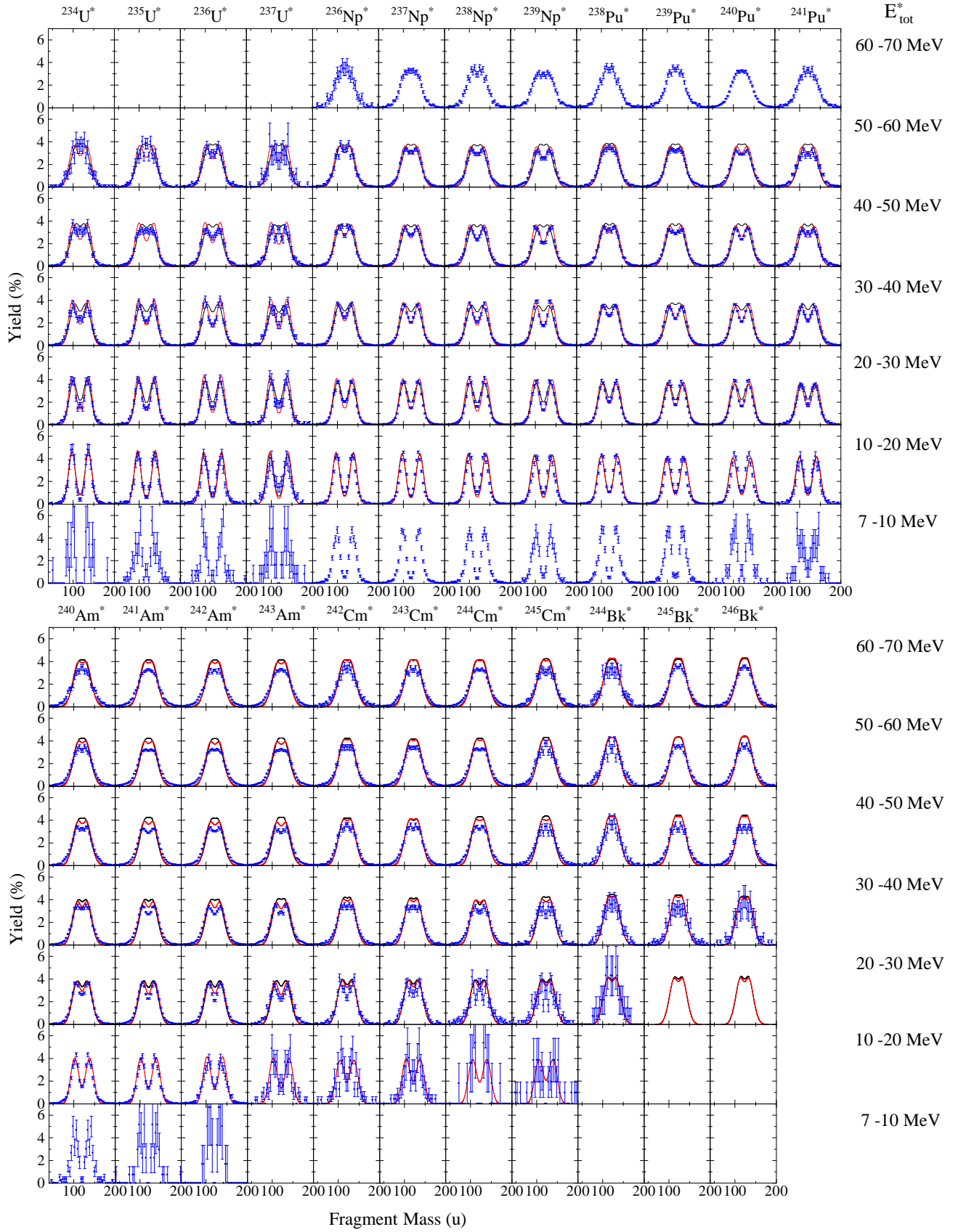
FIG. 3: (Color online) Fission fragment mass distributions for $^{234-236}$U*, $^{236-239}$Np*, $^{238-241}$Pu*, $^{240-243}$Am*, $^{242-245}$Cm*, $^{244-246}$Bk*, obtained in the MNT channels of the ^{18}O+^{238}Np reaction. Total excitation energies E^*_{tot} are shown on the right-hand side. Red and black curves are the calculation using the Langevin approach with and without assuming neutron evaporation before fission (multi-chance fission), respectively.

TABLE I: Most probable total excitation energy E^*_{opt} from Eq. (1) in MeV, estimated from the momentum matching condition for each transfer channel in the reaction of ^{18}O+^{237}Np at $E_{\text{c.m.}}$=150.5 MeV. Q_{gg} is the ground state Q-value (in MeV) obtained from the mass table of [27], m and n are the number of transferred nucleons from or to projectile. See Appendix A for explanation of Q_{opt} values. For the channel to give a compound nucleus ^{237}Np, two cases of $m=n=0^{\sharp 1}$ and $m=n=1^{\sharp 2}$ are shown.

Channel	Q_{gg}	(m,n)	$m+n$	Q_{opt}	E^*_{opt}
^{21}F+^{234}U	+5.99	(0,3)	3	−36.69	42.69
^{20}F+^{235}U	+3.19	(0,2)	2	−28.28	31.47
^{19}F+^{236}U	+3.13	(0,1)	1	−16.63	19.76
^{18}F+^{237}U	−2.17	(1,1)	2	−29.95	27.78
^{19}O+^{236}Np	−2.62	(0,1)	1	−16.63	14.00
^{18}O+^{237}Np$^{\sharp 1}$	0.00	(0,0)	0	− 0.00	0.00
^{18}O+^{237}Np$^{\sharp 2}$	0.00	(1,1)	2	−29.95	29.95
^{17}O+^{238}Np	−2.56	(1,0)	1	−17.36	14.81
^{16}O+^{239}Np	−0.48	(2,0)	2	−30.45	29.97
^{17}N+^{238}Pu	−9.95	(1,0)	1	−17.36	7.42
^{16}N+^{239}Pu	−10.18	(2,0)	2	−30.45	20.27
^{15}N+^{240}Pu	−6.14	(3,0)	3	−40.31	34.17
^{14}N+^{241}Pu	+11.73	(4,0)	4	−47.73	36.01
^{15}C+^{240}Am	−17.29	(3,0)	3	−40.31	23.01
^{14}C+^{241}Am	−11.87	(4,0)	4	−47.73	35.87
^{13}C+^{242}Am	−14.50	(5,0)	5	−53.32	38.82
^{12}C+^{243}Am	−13.09	(6,0)	6	−57.52	44.44
^{13}B+^{242}Cm	−27.28	(5,0)	5	−53.32	26.05
^{12}B+^{243}Cm	−26.46	(6,0)	6	−57.52	31.06
^{11}B+^{244}Cm	−23.03	(7,0)	7	−60.68	37.65
^{10}B+^{245}Cm	−28.96	(8,0)	8	−63.04	34.08
^{11}Be+^{244}Bk	−36.80	(7,0)	7	−60.68	23.88
^{10}Be+^{245}Bk	−30.33	(8,0)	8	−63.04	32.71
^{9}Be+^{246}Bk	−31.23	(9,0)	9	−64.81	33.58

should practically conserve that of the $P_{\text{CN}}(E^*)$ distribution.

We consider the MNT reaction $a + A \rightarrow b + B$, i.e. the reaction between projectile (a) and target (A) nuclei resulting in ejectile (b) and the recoiled (B) nuclei, by transferring m nucleons from a to A and n nucleons from A to a. The momentum matching condition [23] gives a optimal Q-value of the reaction Q_{opt}, as shown in Appendix A, from which the most probable total excitation energy E^*_{opt} can be calculated as,

$$E^*_{\text{opt}} = Q_{\text{gg}} - Q_{\text{opt}}, \qquad (1)$$

using the Q-value of ground-to-ground states transition, Q_{gg}. In general E^*_{opt} increase with the total number of exchanging nucleons, $m + n$. Results of the calculation for the ^{18}O+^{237}Np reaction are summarized in Table I. Here, the (m, n) values cannot be uniquely determined. We used the values of least number of exchanged nucleons to produce a particular CN, $\min(m + n)$. In Fig.2, the estimated E^*_{opt} values are shown by the horizontal dash-dotted line in the right-side panel of each nuclide section. It is seen that the calculated E^*_{opt} value increases with the total number of transferred nucleons, thus reproducing the experimentally observed trend (cf. Fig. 2). The most probable excitation energies of the measured spectra, however, show higher values than the calculated ones, for +3p+xn and +4p+xn channels. For uranium isotopes, no clear trend is obtained in experiment in terms of the number of transferred neutrons, in contrast to the calculation that predicts large E^*_{opt} with respect to $m + n$. We also note for the channel ^{18}O+^{237}Np→^{18}O+^{237}Np* that the model without nucleon transfer predicts zero excitation energy as shown by the ♯1 line in Table I. The experimental data, however, shows a significantly high excitation energy. If we assume $m=n=1$ for this channel, E^*_{opt}=29.95 MeV is predicted as shown by the ♯2 line in Table I, and by the horizontal dotted line in Fig. 2. As the largest yield in the E^*_{tot} spectrum for ^{18}O+^{237}Np→^{18}O+^{237}Np* is found at ∼20 MeV, a mixture of $m=n=0$ and $m=n=1$ process would be implied.

B. Fission fragment mass distributions

The FFMDs in Fig. 3 show an interesting trend in terms of their dependence on atomic and mass numbers of the fissioning nucleus.

First of all, we have characterized the measured FFMDs by the light- and heavy-fragment peak positions and the peak-to-valley (P/V) ratio, defined as the ratio of the yield at the asymmetric peak position to the one at symmetric fission. They were determined by fitting the experimental data points around the peak and valley regions with a quadratic function. The obtained P/V ratios are shown in Fig. 4 for the excitation-energy ranges of (a) E^*_{tot}=10–20 MeV, (b) 20–30 MeV, and (c) 30–40 MeV, as the regions where the isotope and excitation energy dependence clearly shows up. In the same fitting procedure we also obtained the light-(L) and heavy-(H) fragment peak positions as shown in Fig. 5.

The P/V ratios at the lowest energy in Fig. 4(a) significantly depend on the atomic number of the fissioning nucleus, by showing the light-element isotopes to have larger values. It is seen from the spectra of Fig. 4(b) and (c) that the P/V ratios decrease with excitation energy, and also exhibit an increasing trend with the mass of the CN for neptunium, plutonium and americium isotopes.

Our measurement revealed an interesting trend in the light- and heavy-fragment peak positions, shown in Fig.5. At the lowest energy in the panel (a), the heavy fragment peak maintains nearly the same value for all the studied nuclides, and mass number A_{H}=136.8 fits almost all the data within uncertainty (see dash-dotted curve). Contrary to the stable heavy-peak position, the average light-fragment mass linearly increases with the CN mass (A_{CN}) with the slope of $\Delta A_{\text{L}}/\Delta A_{\text{CN}}$=1.0, as shown by the dashed curve. However, for the higher excitation energy of E^*_{tot}=30–40 MeV in the panel (c), an inverted trend appears. The heavy fragment peak exhibits a mod-

erately increasing behavior with A_{CN} by showing a clear separation between the neighboring elements, whereas the light-fragment peaks in the same element member sustain the same peak position.

We note that these peak positions do not necessarily indicate the properties of Standard fission mode [28] when FFMD has a relatively large mass-symmetric yield. Presence of symmetric-fission mode automatically moves the peaks of asymmetric-fission to larger mass-asymmetry, which does not coincide with the maximum yield positions that we have determined. It should be also mentioned the possible shift of the peak positions caused by the present mass resolution (σ_A=6.5 u). A simple calculation demonstrates that the peak shift is less than 1 u when the P/V ratio of the original FFMD is larger than 1.7. For the data ^{243,244}Cm at E^*_{tot}=20-30 MeV and ^{240,242}Am at E^*_{tot}=30-40 MeV, having the P/V ratio of 1.1~1.2, the peaks would shift to the symmetric region with about ~3 u. Still this is within the error bars.

To shed a light on the observed trend of the P/V ratio and light- and heavy-fragment peak position, we have performed the Langevin calculations, adopting the formalism described in [3, 12, 13, 20]. Here, we mention only basic model ingredients. Nuclear shape is defined by the two-center shell model parametrization [29, 30], which has three shape parameters z (distance between two potential centers), α (mass asymmetry of fragments), and δ (deformation parameter). Potential energy is defined by the sum of liquid-drop part and the microscopic energy term (shell correction and paring energy). Here, the shell correction energy depends on nuclear temperature (T), determined by multiplying the following factor $\Phi(T)$ to the value at zero-temperature,

$$\Phi(T) = \exp\left(-\frac{a\,T^2}{E_d}\right). \qquad (2)$$

The well-accepted shell damping energy E_d=20 MeV was employed [31]. We adopted the level density parameter a as in [13, 32]. To calculate the potential energy in the two-center shell model, a neck parameter ϵ must be given. We adopted the optimal ϵ value [20] according to the following expression using the mass of a CN (A_{CN}),

$$\epsilon(A_{CN}) = 0.01007 A_{CN} - 1.94. \qquad (3)$$

In the present calculation, we also introduced the multi-chance fission (MCF), i.e. fission after neutron evaporation [2, 3]. By evaporating neutrons prior to fission, fission starts from lower excitation energy than the initial CN. This effect revives the shell energy responsible for mass-asymmetric fission, making the FFMD to have a more pronounced double-humped structure with the larger P/V ratio. To evaluate the probability for each fission chance (1st, 2nd, 3rd,..) a competition between neutron evaporation and fission was calculated using the GEF code [26]. In the MCF process, mass of the fissioning system decreases in accordance with the number of emitted neutrons. To make an easy comparison of the FFMD with the experimental data, we transformed the mass-asymmetry α to fragment masses by using the initial compound-nucleus mass A_{CN}.

For the calculation we assume that all the excitation energy E^*_{tot} available after the MNT reaction is stored only in the fissioning CN. Thus the CN excitation energy becomes $E^* \approx E^*_{tot}$. This assumption is reasonably justified by the first measurement of the excitation of light outgoing-nuclei after the MNT reaction, reported in the reaction of ^{238}U+^{12}C [9] at VAMOS. There, decays from the first excited states of the ejectile niclides, ^{12}C, ^{11}B, and ^{10}Be, were observed with a probability of only 0.12–0.14.

The calculated FFMDs are presented in Fig. 3 with and without including the MCF concept, shown by the red and black lines, respectively. While the former approach explains data well, a clear discrepancy between experimental and theoretical data are seen when MCF is excluded from consideration. These FFMDs exhibit the P/V ratio that rapidly diminishes with excitation energy, and the double-peak structure becomes hardly pronounced already at E^*_{tot}=30–40 MeV for uranium, neptunium and plutonium isotopes, contradicting the experimental data. By including the MCF, the decreasing P/V ratio of FFMD toward the heavier-element isotopes is nicely reproduced, see e.g. the data corresponding to E^*_{tot}=20–30 MeV and 30–40 MeV. These trends involve two ingredients. One is the reduction of the MCF effect due to smaller number of emitted neutrons before fission as discussed in [3], the other is the shrinking of the light- and heavy-fragment peak-position distance.

The P/V ratio and the light- and heavy-fragment peak positions from the calculated FFMDs are compared to the experimental data in Fig. 4 and Fig. 5, respectively. We show only the calculation including the MCF effects. For the P/V ratio, the calculation well reproduce the rapidly decreasing trend toward the heavier atomic number of the CN at the low-excitation energy of E^*_{tot}=10–20 MeV, whereas at the higher energies of 20–30 MeV and 30–40 MeV the increase of the P/V ratio with the CN mass for each element is explained.

Concerning the light- and heavy-fragment peak positions in Fig. 5, the calculation well reproduces the experimental data. The behavior of the light- and heavy-fragment positions with excitation energy can be explained by the effects of MCF. Toward high excitation energies, the FFMD tends to approach a single Gaussian shape due to smearing of the shells. This makes the light- and heavy-fragment peaks to shift to the symmetric-fission. On the other hand, emission of neutrons revives the shells of a nucleus, which acts as keeping the peak position. A number of evaporated neutrons before fission, ν_{pre}, has a close correlation with the neutron binding energy as shown in TABLE I of [3]; CN with lower neutron binding energy has larger ν_{pre}. For a certain atomic number of CN (Z_{CN}), ν_{pre} is larger for heavier-mass isotope. For a fixed mass number (A_{CN}), the heavier element has

smaller ν_{pre} values. Thus, the trend of the peak positions in Fig. 5 with the total excitation energy E_{tot}^* can be explained by the $\nu_{\text{pre}}(Z_{\text{CN}}, A_{\text{CN}})$.

In the data analysis we always adopted the initial compound nucleus mass A_{CN} to be conserved in the masses of both fragments, as we cannot experimentally determine the number of emitted neutrons on the event-by-even basis. A possible shift of the light- and heavy-fragment peak positions generated in this assumption is estimated to be small; 1.3 u and 1.8 u, respectively, for fission of ^{237}U*(E_{tot}^*=55 MeV) having the largest ν_{pre}-value of 3.06 studied in this experiment (ν_{pre} is given in TABLE I of [3]).

In order to have a hint on the angular momentum given in the present MNT reaction, we also carried out a calculation of the FFMD by changing the initial spins of CN from 0 $\hbar$, which was used in the calculation shown in Fig. 3. Larger spins will increase the fission probability competing with neutron evaporation, as demonstrated in the GEF code, thus the FFMD at high-excitation energy will be altered accordingly. For the discussion we use the data of fissioning nucleus ^{238}U*, taken in our previous MNT experiment of ^{18}O+^{238}U in [2], where enough statistics up to E_{tot}^*=60 MeV is available. As shown in Fig. 6 the calculation for 0 $\hbar$ gives better agreement with the experimental data, and the results deviate for spins higher than 20 $\hbar$. This is more clearly examined in Fig. 7, where the change of the calculated (a) P/V ratio and (b) light- and heavy-fragment peak positions are shown. We consider the angular momentum smaller than 20 $\hbar$ is the common characteristic to other MNT channels of the ^{18}O+^{237}Np reaction populating uranium, neptunium, and plutonium isotopes, as the Langevin calculation with 0 $\hbar$ shown in Fig. 3 reproduce the experimental data up to $E_{\text{tot}}^* \sim$55 MeV. For americium nuclides, the same is confirmed in the spectra of E_{tot}^*=20–40 MeV. For the CN of curium and berkelium isotopes, the calculation with and without the MCF reaches closer with each other, so that quantitative discussion on angular momentum cannot be given in the present data. Angular momentum in such a large number of transferring nucleons can be studied with a reaction involving lighter target to produce CN with smaller Z_{CN} which still has large MCF effect.

C. FFMDs from different MNT channels leading to the same CN

Systematic fission studies made at the JAEA with the MNT reaction technique using the ^{18}O beam and different actinide targets allow us for a direct comparisons of the FFMDs for a number of nuclei produced in different transfer channels. In Fig. 8, FFMDs from the present work for nuclides $^{235-237}$U*, ^{239}Np*, and ^{241}Pu* (blue circles) are compared to those from the reactions of ^{18}O+^{232}Th (green rectangles) [1] and the ^{18}O+^{238}U (red triangles) [2]. For all the nuclei and the mea-
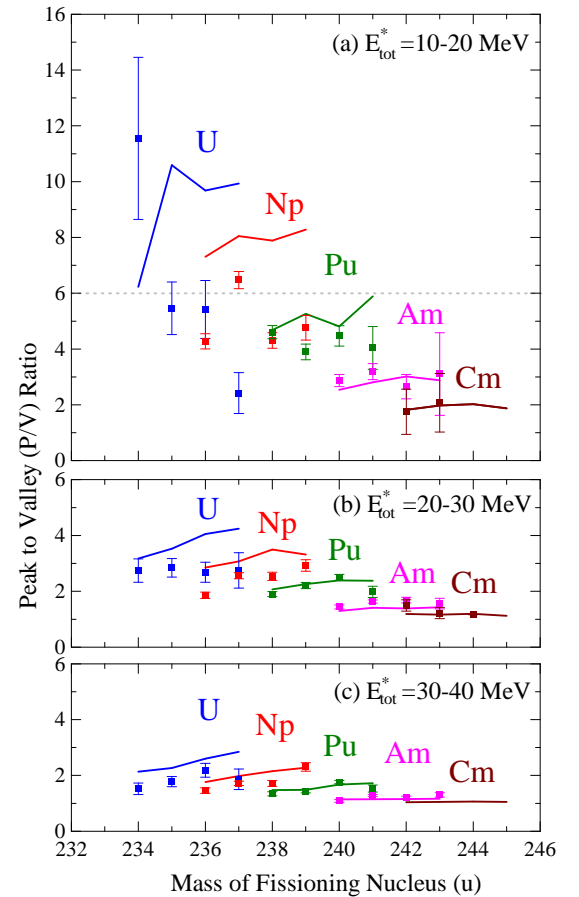

FIG. 4: (Color online) Peak-to-valley (P/V) ratios of the FFMDs for uranium, neptunium, plutonium, americium, and curium isotopes (solid rectangle with error bar), obtained from the measured FFMDs in Fig. 3 for three excitation-energy ranges, (a) 10–20 MeV, (b) 20–30 MeV, and (c) 30–40 MeV. The lines are from the Langevin calculation.

sured excitation energies, general shape of the FFMD remains apparently insensitive to the number of transferred nucleons, i.e., insensitive to the way the CN is produced. In particular, a good agreement of the light- and heavy-fragment peak positions for excitation energies up to E_{tot}^*=35~45 MeV can be noticed, as shown in Fig. 9. Looking at exact detail in fission of $^{235-237}$U*, small difference is seen in terms of the yields in symmetric fission and the maximum yield in the range of 10<E_{tot}^*<40 MeV. This is more quantitatively found in Fig. 9, where the P/V ratios obtained from the FFMDs of Fig. 8 are given. For example, fission of ^{235}U* and ^{236}U* from the ^{18}O+^{237}Np reaction leads to a larger P/V ratio than the one obtained from the ^{18}O+^{232}Th reaction [1] in the excitation energy range 10<E_{tot}^*<40 MeV. For ^{237}U*, on the contrary, the P/V ratio from ^{18}O+^{237}Np is systematically smaller than the reaction ^{18}O+^{238}U up to E_{tot}^*=50 MeV. Thus, for some nuclei, the difference in the P/V ratio is observed already at low excitation energies of 10–20 MeV. At low excitation energy, the MCF effect
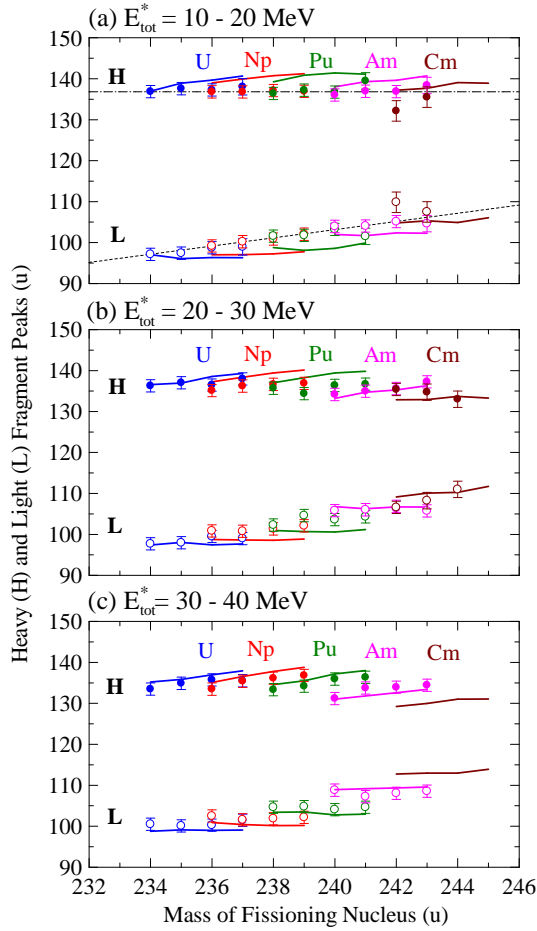
FIG. 5: (Color online) Light(L)- and heavy(H)-fragment peak positions (open and solid circles, respectively) of the fission-fragment mass distributions derived from Fig. 3 for uranium to curium isotopes, as a function of mass of fissioning nucleus and for excitation-energy bins: (a) 10–20 MeV, (b) 20–30 MeV, and (c) 30–40 MeV. The solid lines are the Langevin calculation. In the panel (a), the dash-dotted curve is the best fit value for all the heavy-fragment data, and the dashed line is the fit to the light fragment group.

is not important, thus the results may be associated with the fission mechanism. One of the plausible explanation could be due to different angular momenta given to the CN, depending on the number of transferred nucleons. This is implied in the fission fragment angular distribution relative to the rotational axis of CN, found in the present setup [33]. To produce ^{235}U* and ^{236}U*, three ($+2p+1n$) and four nucleons ($+2p+2n$) must be moved from ^{18}O to ^{232}Th, respectively, whereas two ($-1p-1n$) and one nucleon ($-1p$) is transferred from ^{237}Np to ^{18}O. Among three reactions to produce ^{237}U*, the reaction using the ^{238}U target has the minimum number of transferred nucleons ($-1n$), in comparison to the other two, ^{18}O+^{237}Np ($-1p+1n$) and ^{18}O+^{232}Th ($+2p+3n$). In the Lanvevin calculation [34] for fission of ^{240}U* at the excitation energy of 10 MeV, a small enhancement of the symmetric-fission yield with the amount of $\sim$1.0–1.3 %
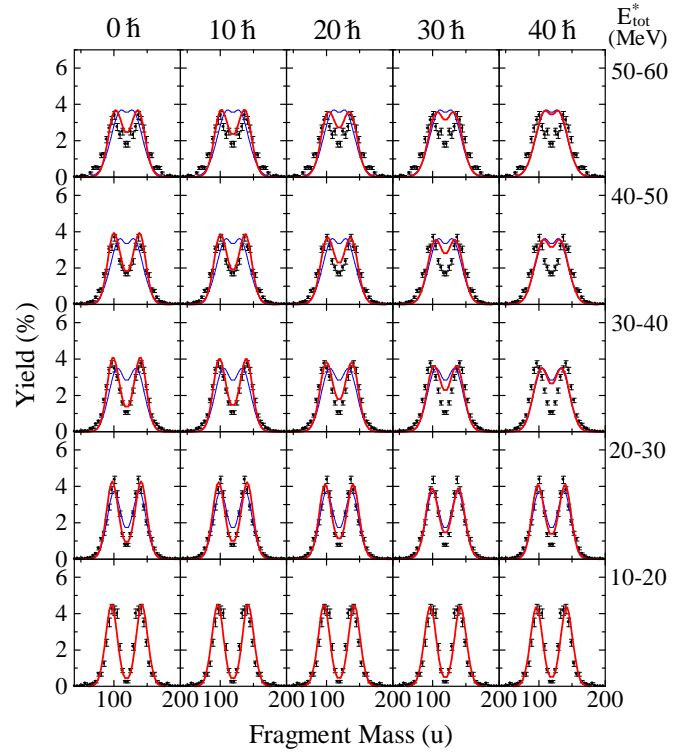

FIG. 6: (Color online) FFMDs and their evolution with the total excitation energy (shown on the right-hand side) for ^{238}U* calculated by the Langevin model (thick red curves), to the experimental data (solid circles with error bars) [2]. Angular momentum of the compound nucleus introduced to calculate the competition between neutron emission and fission in the multi-chance fission process is shown on the top of each column. Calculation excluding the MCF effect is shown by the thin blue curve.

is predicted by changing the spins from 0 to $\sim$10–20 $\hbar$. Considering the difference up to only about $\sim$1.0% in the symmetric fission yield of $^{235-237}$U* at E^*_{tot}=10–20 MeV, detected as the largest difference, the experimental data indicate the angular-momentum difference of about 10 $\hbar$. This difference would be preserved to a CN with high excitation-energy, implied from the observed difference in the symmetric-fission yield of $\sim$0.5 % (see FFMDs of $^{235-237}$U* at E^*_{tot}=30–40 MeV in Fig. 8), which is equally predicted when the angular momentum difference 10 $\hbar$ is adopted in the Lanvegin calculation shown in Fig. 6.

IV. SUMMARY

Multi-nucleon transfer channels of the ^{18}O+^{237}Np reaction were used to obtain FFMDs of $^{234-237}$U*, $^{236-239}$Np*, $^{238-241}$Pu*, $^{240-243}$Am*, $^{242-245}$Cm*, and $^{244-246}$Bk*. Among them the low-energy fission data of ^{236}Np, ^{238}Pu, and ^{245}Cm were reported for the first time.

The most probable total excitation energy, revealed from the coincidence spectrum between FFs and ejectile
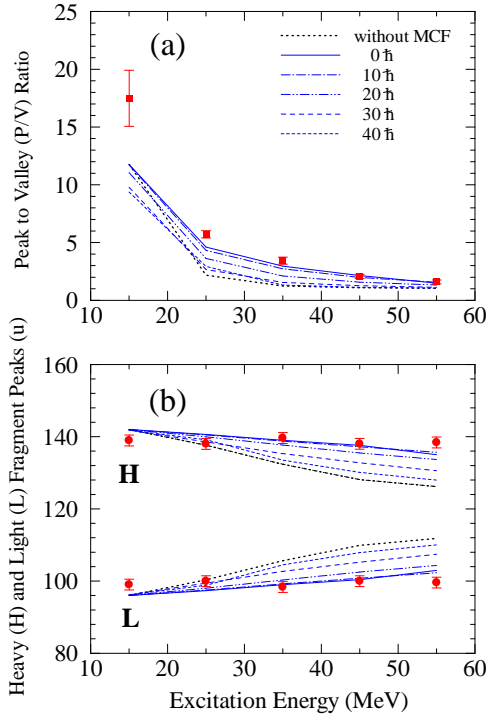
FIG. 7: (Color online) (a) Peak-to-valley (P/V) ratios (solid squares) and (b) light(L)- and heavy(H)-fragment peak positions (solid circles), for fission of ^{238}U [2], are shown as a function of excitation energy. Blue lines with different styles are the results from Lanvevin calculation using the different angular momentum, from 0 to 40 $\hbar$. Calculation without introducing the MCF is shown by the black dotted curve.

nucleus, tends to increase with the increasing mass and atomic number of fissioning nucleus. This general feature can be explained on the basis of the optimal reaction Q-value estimated from the momentum matching condition when the number of transferred nucleons is not larger than ∼6.

FFMDs of all the studied nuclides are found to show a pronounced double-humped structure with mass asymmetric fission at low excitation energies. This structure gradually evolves to the mass-symmetric one when moving to higher excitation energies. The change in the FFMD is addressed by the peak-to-valley (P/V) ratio and the light- and heavy-fragment peak positions. They showed a clear trend in terms of the mass and atomic number of CN. The measured FFMDs are reproduced by the Langevin calculation only if the effects of MCF is introduced. The results also support the assumption that all the excitation energy available after the MNT reaction is stored only in the fissioning CN. From the results angular momentum given in the CN is suggested to be smaller than 20 $\hbar$.

The effect of different transfer channels on the FFMDs was examined using three ^{18}O-induced MNT reactions involving ^{232}Th, ^{238}U, and ^{237}Np as target nuclei. The FFMD data for the nuclei produced with different tar-

get were found to generally agree with each other for all studied excitation-energy ranges. A tiny difference observed in the symmetric-fission yield would be due to the population of different angular momentum, which might depend on the number of transferred nucleons.

V. ACKNOWLEDGEMENT

APPENDIX A: OPTIMAL Q-VALUE IN THE MNT REACTION

The calculation procedure to determine the optimal Q-value Q_{opt} in the MNT reaction is shown [23]. We consider the MNT reaction $a + A \rightarrow b + B$, where a reaction between projectile (a) and target (A) nuclei results in ejectile (b) and the recoiled (B) nuclei, by transferring m nucleons from a to A and n nucleons from A to a. Then the relation $a - m \equiv b - n$ holds. At the point of closest approach, the momentum matching conditions requires the relation,

$$\overrightarrow{p_a} - \overrightarrow{p_m} = \overrightarrow{p_b} - \overrightarrow{p_n}. \tag{A1}$$

Here $\overrightarrow{p_m}$ and $\overrightarrow{p_n}$ are the momenta of the transferred nucleons, represented using the momenta of a ($\overrightarrow{p_a}$) and A ($\overrightarrow{p_A}$),

$$\overrightarrow{p_m} = (m/a)\overrightarrow{p_a}, \quad \overrightarrow{p_n} = (n/A)\overrightarrow{p_A}. \tag{A2}$$

The kinetic energy loss is determined using the initial (i) and final (f) kinetic energies, $\epsilon_i = p_a^2/2\mu_i$ and $\epsilon_f = p_a^2/2\mu_f$,

$$\Delta\epsilon = \epsilon_f - \epsilon_i = -(\sin^2 \beta)\epsilon_i \tag{A3}$$

where $\mu_{i,f}$ are the reduced mass of the entrance and exit channels. Using incident projectile energy in the c.m. frame (E_i) and Coulomb energy (V_i^c) at the closed distance that multi-nucleon transfer process dominate, the optimal Q-value (Q_{opt}) is determined using $\epsilon_i = E_i - V_i^c$

$$Q_{opt} = -(\sin^2 \beta)[E_i - V_i^c], \tag{A4}$$

where

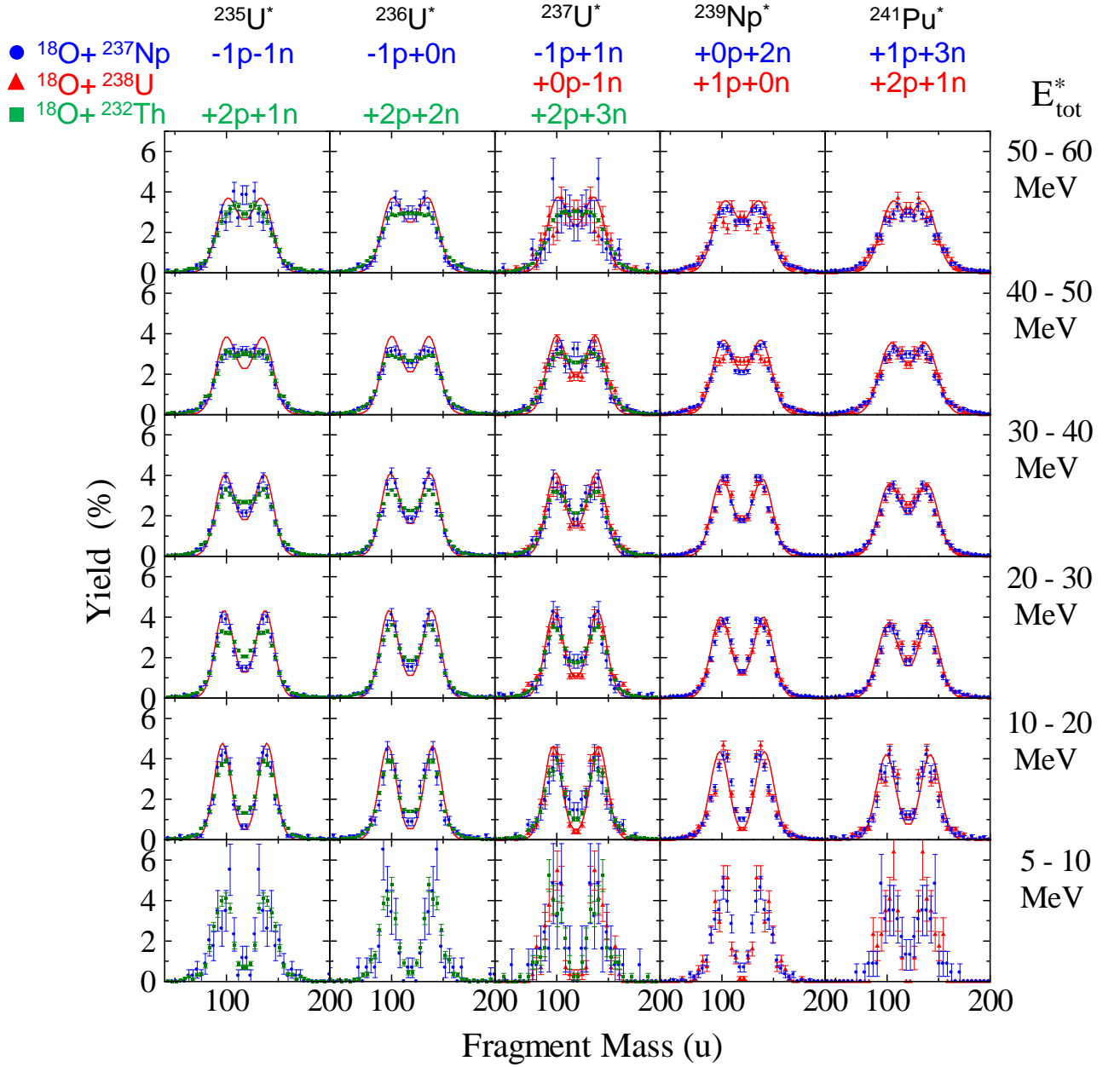$$\cos^2 \beta = 1 - \sin^2 \beta = (1 - \frac{m}{a} - \frac{n}{A})(1 - \frac{m}{B} - \frac{n}{b}). \tag{A5}$$

FIG. 8: (Color online) Fission-fragment mass distribution for $^{235-237}U^*$, $^{239}Np^*$, and $^{241}Pu^*$ obtained in the present $^{18}O+^{237}Np$ reaction (blue circles) are compared to that from the MNT channels in $^{18}O+^{232}Th$ [1] (green squares) and $^{18}O+^{232}U$ [2] (red triangles). The number of transferred neutrons and protons is shown for each CN on the upper part, where positive sign means the movement of nucleon from the projectile to the target nucleus and the negative sign represents the opposite direction. Total excitation-energy (E_{tot}^*) ranges are shown on the right-hand side. Solid curves are the Langevin calculation including the MCF process.

Coulomb barrier V_i^c was calculated to be $81.08\,\mathrm{MeV}$ for the $^{18}O+^{237}Np$ reaction using the expression $V_i^c = Z_1 Z_2 e^2/[r_0(A_1^2 + A_2^2)]$ with $r_0=1.5\,\mathrm{fm}$ [23]. For a reaction using heavy target and relatively small projectile mass, the approximation

$$\sin^2 \beta \simeq 1 + \frac{m}{a} + \frac{n}{b}, \qquad (A6)$$

holds. It means from Eq.(A4) that $|Q_{opt}|$ value increases with the total number of exchanging nucleons $m + n$. The optimal Q-value becomes more realistic by introducing a friction effect [23]. Using the friction parameter α, Q_{opt} value is represented by

$$Q_{opt} = -[1 - \cos^2 \beta \exp(-\alpha \sin^2 \beta)]\epsilon_i. \qquad (A7)$$

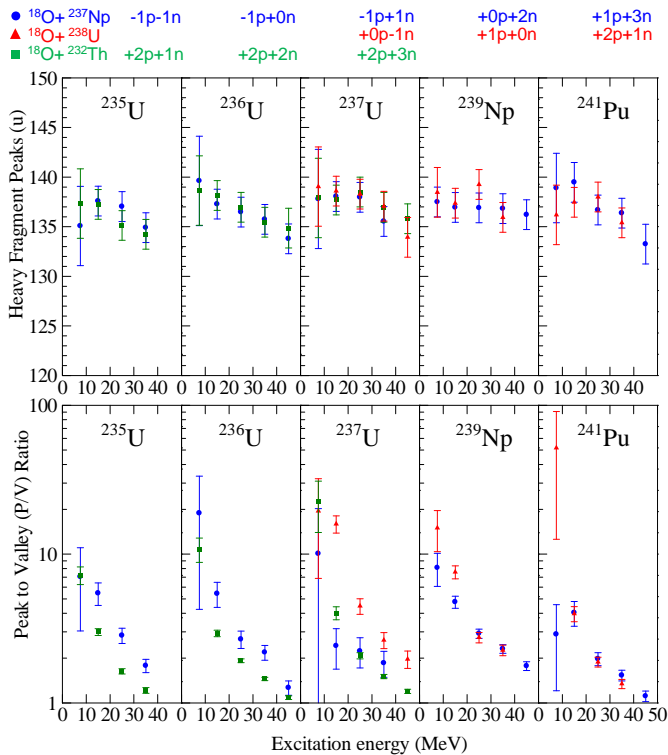Here, we use the α parameter of 3.8 in the present calculation to give better agreement with experiment. Finally,

FIG. 9: (Color online) Heavy-fragment peak positions (upper panels) and the peak-to-valley (P/V) ratios of the FFMDs for $^{235-237}$U*, ^{239}Np*, and ^{241}Pu* as a function of total excitation energy (E^*_{tot}). The data are from the present ^{18}O+^{237}Np reaction (blue circles), ^{18}O+^{232}Th [1] (green squares) and ^{18}O+^{232}U [2] (red triangles). The number of transferred neutrons and protons is shown for each CN on the upper part, see caption of FIG. 8.

we can calculate the most probable total excitation energy E^*_{opt} by the expression Eq. (1) in Section III A.

[1] R. Léguillon, K. Nishio, K. Hirose, H. Makii, I. Nishinaka, R. Orlandi, K. Tsukada, J. Smallcombe, S. Chiba, Y. Aritomo, T. Ohtsuki, R. Tatsuzawa, N. Takaki, N. Tamura, S. Goto, I. Tsekhanovich, C.M. Petrache, and A.N. Andreyev, Phys. Lett. B **761**, 125 (2016).

[2] K. Hirose, K. Nishio, S. Tanaka, R. Léguillon, H. Makii, I. Nishinaka, R. Orlandi, K. Tsukada, J. Smallcombe, M.J. Vermeulen, S. Chiba, Y. Aritomo, T. Ohtsuki, K. Nakano, S. Araki, Y. Watanabe, R. Tatsuzawa, N. Takaki, N. Tamura, S. Goto, I. Tsekhanovich, and A.N. Andreyev, Phys. Rev. Lett. **119**, 222501 (2017).

[3] S. Tanaka, Y. Aritomo, Y. Miyamoto, K. Hirose, and K. Nishio, Phys. Rev. C, **100**, 064605 (2019).

[4] E. Pellereau, J. Taïeb, A. Chatillon, H. Alvarez-Pol, L. Audouin, Y. Ayyad et al., Phys. Rev. C **95**, 054603 (2017).

[5] A. Chatillon, J. Taïeb, H. Alvarez-Pol, L. Audouin, Y. Ayyad, G. Bélier et al., Phys. Rev. C **99**, 054628 (2019).

[6] A. Chatillon, J. Taïeb, H. Alvarez-Pol, L. Audouin, Y. Ayyad, G. Bélier et al., Phys. Rev. Lett. **124**, 202501 (2020).

[7] D. Ramos, M. Caamaño, F. Farget, C. Rodríguez-Tajes,

L. Audouin, J. Benlliure et al., Phys. Rev. C **97**, 054612 (2018).

[8] M. Caamaño, F. Farget, O. Delaune, K.-H. Schmidt, C. Schmitt, L. Audouin et al., Phys. Rev. C **92**, 034606 (2015).

[9] C. Rodríguez-Tajes, F. Farget, X. Derkx, M. Caamaño, O. Delaune, K.-H. Schmidt et al., Phys. Rev. C **89**, 024614 (2014).

[10] M. Caamaño, O. Delaune, F. Farget, X. Derkx, K.-H. Schmidt, L. Audouin et al., Phys. Rev. C **88**, 024605 (2013).

[11] D.C. Hoffman and M.R. Lane, Radiochamica Acta **70/71**, 135 (1995).

[12] Y. Aritomo and S. Chiba, Phys. Rev. C **88**, 044614 (2013).

[13] Y. Aritomo, S. Chiba, and F. Ivanyuk, Phys. Rev. C, **90**, 054609 (2014).

[14] J. Sadhukhan, W. Nazarewicz, and N. Schunck, Phys. Rev. C **93**, 011304(R) (2016).

[15] M.D. Usang, F.A. Ivanyuk, C. Ishizuka, and S. Chiba, Phys. Rev. C **94**, 044602 (2016).

[16] M.R. Pahlavani and S.M. Mirfathi, Eur. Phys. J. **52**, 95 (2016).

[17] A.J. Sierk, Phys. Rev. C **96**, 034603 (2017).

[18] C. Ishizuka, M.D. Usang, F.A. Ivanyuk, J.A. Maruhn, K. Nishio, and S. Chiba, Phys. Rev. C **96**, 064616 (2017).

[19] M.D. Usang, F.A. Ivanyuk, C. Ishizuka, and S. Chiba, Phys. Rev. C **96**, 064617 (2017).

[20] Y. Miyamoto, Y. Aritomo, S. Tanaka, K. Hirose, and K. Nishio, Phys. Rev. C, **99**, 051601(R) (2019).

[21] https://www-nds.iaea.org/RIPL-3/fission/empirical-barriers.dat

[22] K.R. Kean, K. Nishio, K. Hirose, M.J. Vermeulen, H. Makii, R. Orlandi, K. Tsukada, A.N. Andreyev, I. Tsekhanovich, S. Chiba, Phys. Rev. C, **100**, 014611 (2019).

[23] Y. Alhassid, R.D. Levine, J.S. Karp, and S.G. Steadman, Phys. Rev. C **20**, 1789 (1979).

[24] P.J. Siemens, J.P.—Bondorf, D.H.E. Gross, and F. Dickmann, Phys.Lett. **36B**, 24 (1971).

[25] D.M. Brink, Phys. Lett. **40B**, 37 (1972).

[26] K.-H. Schmidt, B. Jurado, C. Amouroux, and C. Schmitt, Nucl. Data Sheets, **131**, 107 (2016).

[27] G. Audi, A.H. Wapstra and C. Thibault, Nucl. Phys. A **729**, 337 (2003).

[28] U. Brosa, S. Grossmann, and A. Müller, Phys. Rep. **197**, 167 (1990).

[29] J. Maruhn and W. Greiner, Z. Phys. **251**, 431 (1972).

[30] K. Sato, A. Iwamoto, K. Harada, S. Yamaji, and S. Yoshida, Z. Phys. A **288**, 383 (1978).

[31] A. V. Ignatyuk, G. N. Smirenkin, and A. S. Tishin, Sov. J. Nucl. Phys. **21**, 255 (1975).

[32] J. Toke and W. J. Swiatecki, Nucl. Phys. A **372**, 141 (1981).

[33] S, Tanaka *et al.,* To be submitted.

[34] S. Chiba, O. Iwamoto, Y. Aritomo, Phys. Rev. C **84**, 054602 (2011).